Ultrasound in Med. & Biol., Vol. 26, Supplement 1, pp. S23–S29, 2000

0301-5629/00/$–see front matter

PII S0301-5629(00)00156-3

● *Part I: Science and Technology*

ELASTOGRAPHIC IMAGING

J. OPHIR,*† B. GARRA,‡ F. KALLEL,* E. KONOFAGOU,* T. KROUSKOP,§ R. RIGHETTI*† and T. VARGHESE*

*Department of Radiology, The University of Texas Medical School, Ultrasonics Laboratory, Houston, Texas, USA; †Department of Electrical Engineering, University of Houston, Houston, Texas, USA; ‡University of Vermont, Burlington, Vermont, USA; and §Baylor College of Medicine, Houston, Texas, USA

INTRODUCTION

The mechanical attributes of soft tissues depend on their molecular building blocks (fat, collagen etc.), on the microscopic and macroscopic structural organization of these blocks (Fung 1981), and on the boundary conditions involved. These mechanical attributes may include the shear or elastic moduli (Young's modulus), the Poisson's ratio, or any of the longitudinal or shear strains that occur in tissues as a response to an applied load. In the normal breast, for example, the glandular structure may be firmer than the surrounding fibrous connective tissue, which in turn is firmer than the subcutaneous adipose tissue. Pathological changes are generally correlated with changes in tissue stiffness as well. Many cancers, such as scirrhous carcinomas of the breast, seem much stiffer and less mobile than benign (fibroadenoma) tumors (Anderson 1953). In many cases, in spite of the difference in stiffness or mobility, the small size of a pathological lesion and/or its location deep in the body impede its detection and/or evaluation by palpation. Moreover, lesions may or may not possess echogenic attributes that make them ultrasonically detectable. Because the echogenicity and the mechanical attributes of tissue are generally uncorrelated, it is expected that imaging some of the latter will provide new information that is related to tissue structure and/or pathology. For example, tumors of the prostate or the breast may be invisible or barely visible in standard ultrasound examinations, yet are much stiffer than the embedding tissue. Diffuse diseases such as cirrhosis of the liver are known to increase the stiffness of the liver tissue significantly (Anderson 1953), yet they may seem normal in conventional ultrasound examination. A clear understanding of tissue stress/strain relationships is necessary for the interpretation of any of these imaged mechanical attributes.

Tissue may exhibit viscoelastic and poroelastic behavior such as hysteresis, fluid flow, stress relaxation and creep (Fung 1981). When all these factors are combined, it is evident that describing the mechanical behavior of tissue mathematically requires considerable simplification, if the model is to be useful in a real-time or nearly real-time situation. To a first approximation, most soft tissues have been assumed to be isotropic on the scale of interest (Krouskop et al. 1987; Parker et al. 1990; Sarvazyan et al. 1991), although there is evidence of anisotropic ultrasonic and mechanical attributes in some soft tissues such as muscle (Levinson 1987). Even for relatively small strains (less than 10%), tissue may exhibit nonlinear viscoelastic behavior (Krouskop et al. 1998; Parker et al. 1990). Thus, the mechanical attributes of tissue are often better defined if they are specified over the strain or stress ranges of interest in a specific application (Krouskop et al. 1987; Levinson 1987; Parker et al. 1990).

Quantitative measurements of tissue mechanical parameters reported in the past show a wide range of values (Fung 1981; Parker et al. 1990). Most of the research has been done for tissues that undergo tensile loading (muscles, arteries, lung, tendons, bone, skin, ureter). In contrast, very little quantitative information has been collected on the compressive attributes of the tissue in organs. A limited set of *in vitro* measurements of the elastic moduli of prostate and liver tissues was described by Parker et al. (1990). In a presentation by Sarvazyan (1993), shear modulus measurements indicated that normal breast tissue is approximately 4 times less stiff than fibroadenoma. Breast cancer showed a wide range of shear moduli that can be up to 7 times higher than those of normal tissue. Walz et al. (1993) presented results of

Address correspondence to: Dr. Jonathan Ophir, Ultrasonics Laboratory, Radiology Department, The University of Texas, Medical School, 6431 Fannin Street, Suite 6.168, Houston, TX 77030, USA. E-mail: jonathan.ophir@uth.tmc.edu.

an *in vivo* study involving 250 breast lesions, which indicated that fibroadenomas are approximately 8 times softer than carcinomas. Krouskop et al. (1998) measured the compressive moduli of normal and cancerous breast and prostate tissues *in vitro*, demonstrating several-fold increases in the moduli of malignant tissues compared to normal tissues, as well as a distinct nonlinear stress/strain behavior in the tumors.

APPROACHES TO ELASTOGRAPHIC IMAGING

The existence of such significant differences in the responses of abnormal and normal tissue to mechanical stimuli bode well for continued development of imaging techniques that display various mechanical attributes of the tissues of interest. At present, there are several schools of thought about how the mechanical attributes can be best displayed to provide the most useful diagnostic information. One class of techniques (sonoelasticity imaging) involves the application of low-frequency vibrational energy to the tissue, and the simultaneous ultrasonic Doppler detection of ultrasonic waves that have been perturbed by the vibrations (Krouskop et al. 1987; Parker et al. 1990; Yamakoshi et al. 1990). The resulting image displays the elastic modulus calculated from the local wavelength of the shear-wave, or the amplitude of the vibration that is related to the shear modulus. Another approach, termed elastography (Ophir et al. 1991), involves the imaging of the local responses of the medium (or tissue) to an applied load (a common practice by structural engineers), by imaging the longitudinal or shear-strain components produced by this load at different locations in the tissue. The load is applied to the tissue in stepwise increments, with the measurements being made after the motion has essentially ceased. The resultant image is known as an elastogram. In this article, we refer generically to images of any mechanical attributes of tissue as "elastograms." The third school of thought involves a further step of reconstruction of the elastic moduli from the displacement or strain data obtained through elastography (Kallel et al. 1996; O'Donnell et al. 1994; Sumi et al. 1995).

Depending on the mechanical attributes to be imaged, the aforementioned approaches may be classified into two distinct groups. In the first group, the imaged mechanical attributes are based on a direct estimation of one or more parameters from experimental observations. For example, in the case of elastography, the parameters to be imaged are the longitudinal strains, the shear strains or the Poisson's ratio (Ophir et al. 1999) estimated from pre- and postcompression ultrasonic data. In the second group, the mechanical attribute to be imaged is based on an indirect estimation of one or many parameters obtained through the solution of an inverse problem using directly estimated data and a mechanical forward model of the tissue. For example, in the case of elastography, the mechanical attribute to be reconstructed and imaged is the static shear modulus obtained using some estimated components of the 3-D tissue strain field and assuming the tissue to behave as a linear, isotropic, incompressible elastic material at the scale of interest.

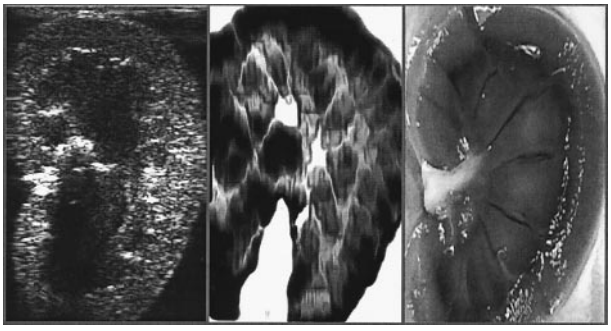

Fig. 1. Longitudinal ovine kidney *in vitro*. (Left) Sonogram. Observe poor SNR in the sinus area and distal shadowing. (Center) Elastogram (black corresponds to low strain and the white to high strain). The strain estimates obtained in regions where the sonographic SNR is low are shown to contain a wealth of detail. This elastogram is obtained following a single (0.5%) compression. Scans were obtained at 5 MHz. The elastogram demonstrates structures that are consistent with a hard renal cortex and medullary pyramids (of which at least seven are seen), softer columns of Bertin, and very soft areas at the base of the columns. (Right) These structures are also seen in the cut pathological specimen. In the elastogram, black = hard; white = soft.

The second group of approaches attempts to calculate and display the static or dynamic shear modulus, which is one of the basic mechanical tissue attributes. These approaches involve many formidable assumptions about the tissue model and the boundary conditions. These assumptions are necessary because of the incomplete knowledge about the tissue behavior and about the boundary conditions at all scales needed to solve the problem. Image quality may also be degraded by the errors that may be introduced by the intense calculations that are generally required. It is, therefore, difficult to measure just how well the final image displays the true moduli.

In the first group of techniques, no assumptions are made because direct measurements are obtained; however, the interpretation of the resulting image may be difficult for certain tissues, because of the presence of elastographic artifacts (Ophir et al. 1999). It is important to note that the measurements obtained from the first group of approaches are used as inputs to the second group of approaches. From the clinical application point

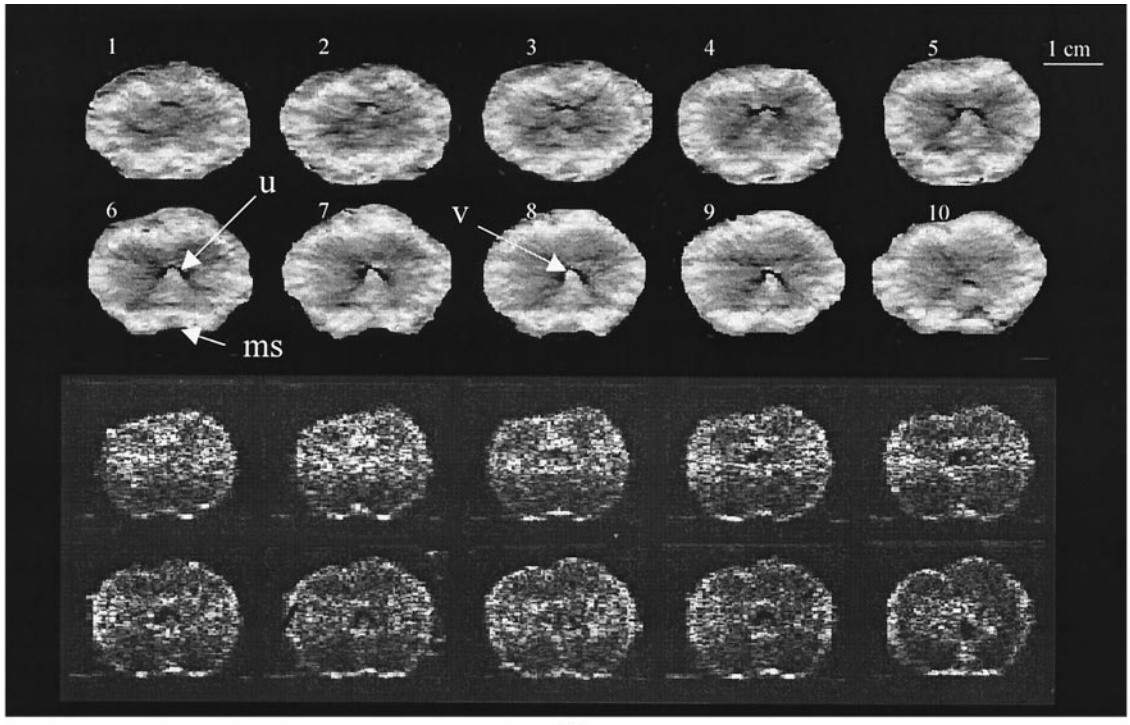

(a)

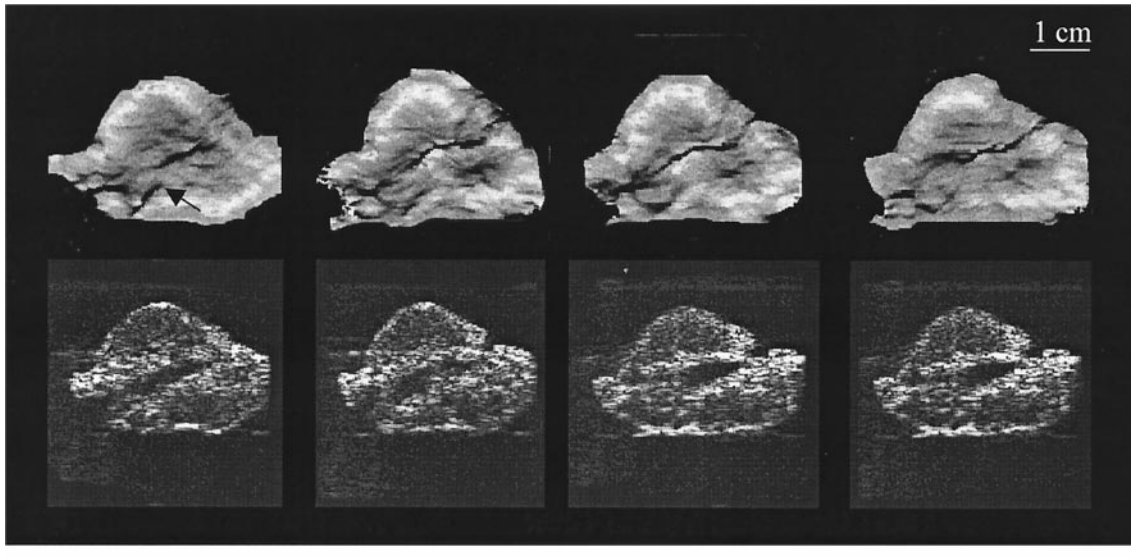

(b)

Fig. 2. (a) Serial cross-sectional view through a canine prostate *in vitro*, obtained with a Diasonics Spectra scanner at 5 MHz. (Top two rows) Elastograms separated by 1-mm increments, progressing from apical to basal views of the gland. In these elastograms, white represents areas of low strain, and black represents areas of high strain. Note the excellent contrast between the outer gland and the inner gland, and the clear visualization of the verumontanum (views 5–9), the urethra (black inverted V) and the network of branching-fibrous connective tissue septae radiating from the urethra to the outer gland. Note the urethra (u), verumontanum (v) and median sulcus (ms). All the elastograms are displayed using the same strain dynamic range of 0–3%. (Bottom two rows) The corresponding sonograms from which the elastograms were derived. (b) Parasagittal views near and at the center of a canine prostate *in vitro*, obtained from a Diasonics Spectra scanner at 5 MHz. (Top row) Axial strain elastograms, where white represents regions of low strain, and black represents regions of high strain. The apex is on the right and the base is on the left. Observe the clear depiction of the urethra and of some of the ducts, the excellent contrast between the outer and the inner gland and the visualization of the verumontanum as a low strain area located at the distal central part of the urethra (two center images). (Bottom row) The corresponding sonograms from which the elastograms were computed. In the elastograms, black = soft; white = hard. (From Kallel et al. 1999b)

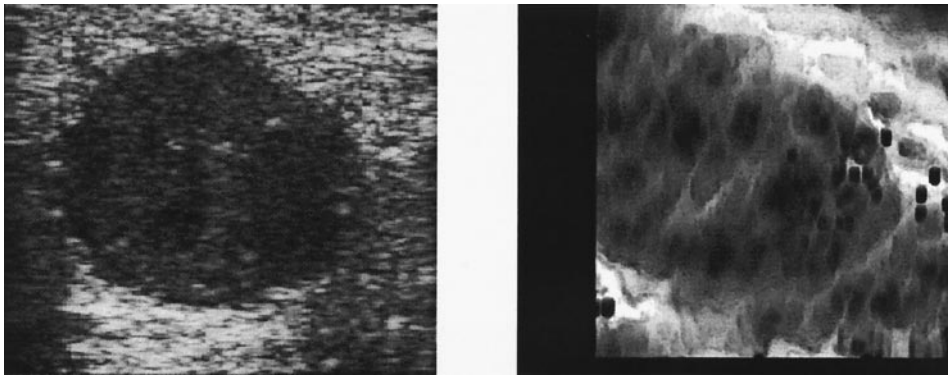

Fig. 3. (Left) Sonogram and (Right) elastogram of a multifocal invasive ductal carcinoma *in vivo*, obtained at 5 MHz. Observe the multiple low strain foci (lack) within the elastographic tumor, some of which correspond to the positions of micro-calcifications in the sonogram. Image width is 40 mm. In the elastogram, black = hard; white = soft.

of view, the value of one approach relative to another is still unknown, because of the paucity of available data.

PRINCIPLES OF ELASTOGRAPHY

Elastography is based on the following assumptions: (1) The load applied to the tissue can be considered to be static. The data acquisition time is so short compared to the time over which loading changes, that the load may be considered to be constant during data acquisition. This minimizes problems because of reflections, standing waves and mode patterns that may interfere with quality image formation during sonoelasticity imaging; (2) the applied load reduces the complexity of the generalized dynamic viscoelastic equation of forced motion to the much simpler Hookean equation; and (3) the strain in the tissue is very small (on the order of 1% or less) and the constitutive equation is considered to be linear.

When an elastic medium is compressed by a constant uniaxial load (stress or displacement), all points in the medium experience a resulting level of longitudinal strain whose principal components are along the axis of compression. If one or more of the tissue elements has a different stiffness parameter than the others, the level of strain in that element will be higher or lower; a stiffer tissue element will generally experience less strain than one which is less stiff. The longitudinal (axial and lateral) strains are estimated from the analysis of ultrasonic signals obtained from standard diagnostic ultrasound equipment. This is accomplished by (1) acquiring a set of digitized radio-frequency echo lines from the tissue region-of-interest; (2) compressing the tissue by a small amount with the ultrasonic transducer (or with a transducer/compressor combination) along the ultrasonic radiation axis; and (3) acquiring a second, postcompression set of echo lines from the same region-of-interest. Con-

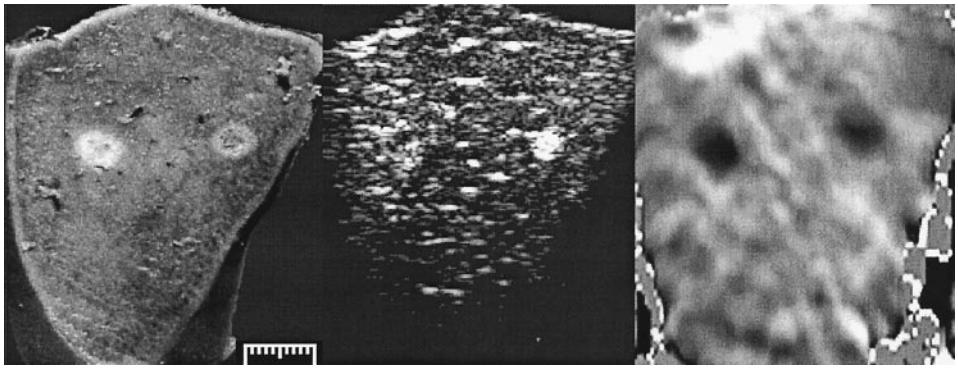

Fig. 4. HIFU-ablated circular regions in a canine liver *in vitro*. (Left) Gross pathological view of a cut surface through the ablated regions. (Center) Sonogram obtained from a Diasonics Spectra scanner at 5 MHz. (Right) The corresponding elastogram, where black represents regions with low strain, and white represents regions with high strain. All views are from approximately the same plane. In the elastogram, black = hard; white = soft.

gruent echo lines that may have been corrected for lateral motion are then subdivided into small temporal windows that are compared pairwise using cross-correlation techniques, from which the change in arrival time of the echoes prior to and following compression can be estimated. Because of the small magnitude of the applied compression, there are only small distortions of the echo lines, and the changes in arrival times are also small. The local axial strain may be estimated as (Ophir et al. 1991):

$$e_{11,\,local} = \frac{(t_{1b} - t_{1a}) - (t_{2b} - t_{2a})}{t_{1b} - t_{1a}}$$

where t_{1a} is the arrival time of the pre-compression echo from the proximal window, t_{1b} is the arrival time of the pre-compression echo from the distal window, t_{2a} is the arrival time of the postcompression echo from the proximal window; and t_{2b} is the arrival time of the postcompression echo from the distal window. The windows are translated in small overlapping steps along the temporal axis of the echo line, and the calculation is repeated for all depths. A similar method is used for lateral strain estimation.

FUTURE TRENDS

Our early hypothesis underlying the efforts to image the strains in soft tissues has been that soft tissue modulus contrast is reliably present, especially between normal and abnormal tissues. Indeed, we have shown that at least two important tissue contrast domains exist. The first is the existence of a large (>20 dB) modulus contrast between normal and some pathological tissues in the breast and in the prostate (Krouskop et al. 1998). The second is the existence of a low (<6 dB) to moderate (<20 dB) modulus contrast even among various normal tissues in the kidney, prostate and breast (Kallel et al. 1998; Krouskop et al. 1998). We have also shown that procedures such as tissue ablation using laser or high intensity focused ultrasound (HIFU) techniques have a profound effect on tissue elastic modulus (Kallel et al. 1999; Righetti et al. 1999; Stafford et al. 1998). These observations, together with some initial clinical observations showing the ability of elastography to detect and characterize sonographically-occult breast cancers (Garra et al. 1997), are providing the catalyst for continuing the vigorous development and application of elastographic methods to medical imaging problems.

The estimation and imaging of tissue strains is by definition a three-dimensional problem. When the tissue is deformed, the near incompressibility of most soft tissue types means that strain tensor components are generated in all directions simultaneously. Until recently, workers in the field had assumed that single-view ultrasonic methods could not be used for precision lateral displacement and strain estimates (Cohn et al. 1997; Kallel 1995; Lubinski et al. 1996). As a result, they were essentially limited to displacement and strain estimations related to the axial direction. Konofagou and Ophir (1998) and Konofagou et al. (1999) have demonstrated that it is possible to make precision estimations of lateral displacements and to produce images of lateral strain and Poisson's ratio distributions in tissues, if proper overlap between adjacent ultrasonic beams is maintained.

Given the existence of significant and reproducible modulus contrast in many normal and abnormal tissues, and the ability to estimate some of the components of the strain tensor, the noise performance of these estimations becomes the important parameter that limits the achievable image quality with which elastograms can be made. A theoretical framework (Varghese and Ophir 1997; Varghese et al. 1998) has been formulated to describe the trade-offs among all the technical parameters of the ultrasound instrumentation and the signal processing, in terms of their influence on the elastographic image parameters (Alam et al. in press; Konofagou et al. 1997a,b; Varghese and Ophir 1997, 1998; Varghese et al. 1998). A similar framework has been described to characterize the lateral strain estimation process (Konofagou 1999). A contrast-transfer efficiency (CTE) function has been derived and theoretically corroborated (Kallel et al. 1996; Ponnekanti et al. 1995). The CTE provides a description based on linear elasticity theory of the efficiency with which actual modulus contrast is converted to elastographic strain contrast for simple targets and under known geometrical boundary conditions. Based on predictions from the CTE function, Kallel et al. (1998) have shown that, for low contrast situations such as in the normal ovine kidney, the strain elastogram is a reasonable representation of the actual modulus elastogram.

Many interesting challenges remain in the development of this new imaging modality. In principle, it should be possible ultimately to generate elastograms in real time, perhaps by reducing the cross-correlation computations to 1-bit hardware operations, which have been shown to be effective (Ophir et al. 1991, 1996, 1997, 1999), or by using fast digital signal processing (DSP) chips. Precise corrections for lateral and out-of-plane linear motions seem feasible (Chaturvedi et al. 1997, 1998; Konofagou and Ophir 1998), as do incoherent, direct strain estimation techniques (Konofagou et al. 1999). These approaches are powerful in that they seem effective even when strong decorrelation noise is introduced because of excessive and/or undesired motion (Kallel and Ophir 1997). The optimal elastographic protocols that are to be followed are, as yet, unknown. The amount of pre-compression, the applied imaging compression, the number of sonographic frames and the

(adaptive) algorithm(s) to be used for image optimization, and the relationship of these protocols to the specific mechanical attributes (such as contrast and nonlinear stress/strain behavior) of the tissues have yet to be defined. Whereas elastographic artifacts are fairly well understood (Ophir et al. 1996, 1997, 1999), their ambiguous role as detractors or facilitators of lesion detection and/or diagnosis remains unknown. The role of the inverse problem treatment of elastograms (Kallel and Bertrand 1996; Skovoroda et al. 1995; Sumi et al. 1995), and the related definition of tissue moduli at different spatial scales and under variable boundary conditions, remains obscure. Related techniques, such as high-frequency, high-resolution methods (de Korte et al. 1997; Ryan and Foster 1997) applied intravascularly may also develop as useful adjuncts to the current sonographic methods. Finally, direct and incoherent spectral strain estimators may be able to overcome some of the past limitations on the practice of elastography in noisy environments, such as in hand-held or abdominal applications (Konofagou et al. 1999; Varghese et al. submitted; Wilson and Robinson 1982).

CONCLUSIONS

Whereas elastography has progressed rapidly in the past several years, much progress has yet to be made for elastography to achieve the goal of becoming a viable clinical tool. The current promise of elastography lies in the fact that it is theoretically and practically possible to obtain quality images of some of the mechanical attributes of the tissue under an applied load, and that reliable modulus contrast has been demonstrated in several normal and pathological tissues. Even at this early stage in the development of elastography, it is evident that there exists a fortunate set of favorable biological, mechanical, acoustical and statistical conditions that, when combined, bode well for a realistic attainment of this goal.

REFERENCES

Alam SK, Ophir J, Varghese T. Elastographic axial resolution criteria: An experimental study. IEEE Trans Ultrason Ferroelect Freq Contr 2000;47:304–309.

Anderson WAD. Pathology. St Louis: Mosby, 1953.

Chaturvedi P, Insana MF, Hall T, Bilgen M. 3D companding using linear arrays for improved strain imaging. IEEE Ultrason Symp 1997:1435–1438.

Chaturvedi P, Insana M, Hall TJ. 2D companding for noise reduction in strain imaging. IEEE Trans Ultrason Ferroelect Freq Contr 1998;45:179–191.

Cohn NA, Emelianov SY, Lubinski MA, O'Donnell M. An elasticity microscope. Part I: Methods. IEEE Trans Ultrason Ferroelect Freq Contr 1997;44:1304–1318.

de Korte CL, Céspedes EI, van der Steen AFW, Lancee CT. Intravascular elasticity imaging using ultrasound: Feasibility studies in phantoms. Ultrasound Med Biol 1997;23:735–746.

Fung YC. Biomechanical properties of living tissues (Chap. 7). New York: Springer Verlag, 1981.

Garra BS, Céspedes EI, Ophir J, et al. Elastography of breast lesions: Initial clinical results. Radiology 1997;202:79–86.

Kallel F. Proprietes elastiques des tissus mous a partir de l'analyse des changements spatio-temporels dans les signaux ultrasonores. PhD dissertation, Ecole Polytechnique, University of Montreal, 1995.

Kallel F, Bertrand M. Tissue elasticity reconstruction using linear perturbation method. IEEE Trans Med Imag 1996;15:299–313.

Kallel F, Ophir J. Three dimensional tissue motion and its effects on image noise in elastography. IEEE Trans Ultrason Ferroelect Freq Contr 1997;44:1286–1296.

Kallel F, Bertrand M, Ophir J. Fundamental limitations on the contrast-transfer efficiency in elastography: An analytic study. Ultrasound Med Biol 1996;22:463–470.

Kallel F, Ophir J, Magee K, Krouskop T. Elastographic imaging of low-contrast elastic modulus distributions in tissue. Ultrasound Med Biol 1998;24:409–425.

Kallel F, Stafford RJ, Price RE, et al. The feasibility of elastographic visualization of HIFU-induced thermal lesions in soft-tissues. Ultrasound Med Biol 1999a;25:641–647.

Kallel F, Price RE, Konofagou EE, Ophir J. Elastographic imaging of the normal canine prostrate. Ultrason Imag 1999b;21:201–215.

Konofagou EE, Ophir J. A new elastographic method for estimation and imaging of lateral displacements, lateral strains, corrected axial strains and Poisson's ratios in tissues. Ultrasound Med Biol 1998; 24:1183–1199.

Konofagou EE, Ophir J, Kallel F, Varghese T. Elastographic dynamic range expansion using variable applied strains. Ultrason Imag 1997a;19:145–166.

Konofagou EE, Varghese T, Ophir J. Variable compressions with RF and baseband processing for dynamic range expansion of elastograms. J Med Ultrason 1997b;24:753–760.

Konofagou EE, Varghese T, Ophir J, Alam SK. Power spectral strain estimators in elastography. Ultrasound Med Biol 1999;25:1115–1124.

Konofagou EE. 1999 PhD dissertation, University of Houston, Department of Electrical Engineering.

Krouskop TA, Vinson S, Goode B, Dougherty D. A pulsed Doppler ultrasonic system for making noninvasive measurements of the mechanical properties of soft tissue. J Rehab Res Dev 1987;24:1–8.

Krouskop TA, Wheeler TM, Kallel F, Garra BS, Hall T. The elastic moduli of breast and prostate tissues under compression. Ultrason Imag 1998;20:151–159.

Levinson SF. Ultrasound propagation in anisotropic soft tissues: The application of linear elastic theory. J Biomech 1987;20:251–260.

Lubinski AM, Emelianov SY, Raghavan KR, et al. Lateral displacement estimation using tissue incompressibility. IEEE Trans Ultrason Ferroelect Freq Contr 1996;43:247–256.

O'Donnell M, Skovoroda AR, Shapo BM, Emelianov SY. Internal displacement and strain imaging using ultrasonic speckle tracking. IEEE Trans Ultrason Ferroelect Freq Contr 1994;41:314–325.

Ophir J, Céspedes EI, Ponnekanti H, Yazdi Y, Li X. Elastography: A quantitative method for imaging the elasticity of biological tissues. Ultrason Imag 1991;13:111–134.

Ophir J, Céspedes I, Garra B, et al. Elastography: Ultrasonic imaging of tissue strain and elastic modulus *in vivo*. Eur J Ultrasound 1996;3:49–70.

Ophir J, Kallel F, Varghese T, et al. Elastography: A systems approach. Int J Imag Syst Tech 1997;8:89–103.

Ophir J, Alam KA, Garra B, et al. Elastography: Ultrasonic estimation and imaging of the elastic properties of tissues. J Eng Med 1999; 213:203–233.

Parker KJ, Huang SR, Musulin RA, Lerner RM. Tissue response to mechanical vibrations for sonoelasticity imaging. Ultrasound Med Biol 1990;16:241–246.

Ponnekanti H, Ophir J, Huang Y, Céspedes, I. Fundamental mechanical limitations on the visualization of elasticity contrast in elastography. Ultrasound Med Biol 1995;21:533–543.

Righetti R, Kallel F, Stafford RJ, et al. Elastographic characterization

of HIFU-induced lesions in canine livers. Ultrasound Med Biol 1999;25:1099–1113.
Ryan LK, Foster FS. Ultrasonic measurement of differential displacement and strain in a vascular model. Ultrason Imag 1997;19:19–38.
Sarvazyan AP. Shear acoustic properties of soft biological tissues in medical diagnostics. J Acoust Soc Am 1993;93:2329.
Sarvazyan AP, Skovoroda A, Vucelic D. Utilization of surface acoustic waves and shear acoustic properties for imaging and tissue characterization (unknown) (abstract). 1991.
Skovoroda AR, Emelianov SY, O'Donnell M. Tissue elasticity reconstruction based on ultrasonic displacement and strain images. IEEE Trans Ultrason Ferroelect Freq Contr 1995;42:747–765.
Stafford RJ, Kallel F, Hazle J, et al. Elastographic imaging of thermal lesions in soft-tissue: A preliminary study *in-vitro.* Ultrasound Med Biol 1998;24:1449–1458.
Sumi C, Suzuki A, Nakayama K. Estimation of shear modulus distribution in soft tissue from strain distribution. IEEE Trans Biomed Eng 1995;42:193–202.
Varghese T, Ophir J. A theoretical framework for performance characterization of elastography: The strain filter. IEEE Trans Ultrason Ferroelect Freq Contr 1997;44:164–172.
Varghese T, Ophir J. An analysis of the elastographic contrast-to-noise ratio performance. Ultrasound Med Biol 1998;24:915–924.
Varghese T, Bilgen M, Ophir J. Multiresolution imaging in elastography. IEEE Trans Ultrason Ferroelect Freq Contr 1998;45:65–75.
Varghese T, Konofagou EE, Ophir J, Alam SK, Bilgen M. Direct strain estimation in elastography using spectral cross-correlation. Ultrasound Med Biol (submitted).
Walz M, Teubner J, Georgi, M. Elasticity of benign and malignant breast lesions, imaging, application and results in clinical and general practice. Eighth International Congress on the Ultrasonic Examination of the Breast, 1993;56.
Wilson LS, Robinson DE. Ultrasonic measurement of small displacements and deformations of tissue. Ultrason Imag 1982;4:71–82.
Yamakoshi Y, Sato J, Sato T. Ultrasonic imaging of internal vibration of soft tissue under forced vibration. IEEE Trans Ultrason Ferroelect Freq Contr 1990;37:45–53.